Earth, Planets and Space
a SpringerOpen Journal

FULL PAPER

Open Access

CrossMark

Characteristics of the atmospheric electric field and correlation with CO_2 at a rural site in southern Balkans

Nikolaos Kastelis[*] and Konstantinos Kourtidis

Abstract

In the current work, 4 years of atmospheric electric field observations at a rural site near Xanthi, Greece, are presented for 2011–2014. The site is situated in an area with very high radon fluxes and high thunderstorm activity. The annual variation is consistent with that at other Northern Hemisphere continental stations, with maxima (minima) occurring during the cold (warm) months. The diurnal variation of the atmospheric electric field both for fair weather (FW) and all weather is found to exhibit a double-peak structure corresponding to local effects and global thunderstorm activity. Comparison with the Carnegie curve shows that nighttime hours and winter months are preferable for observing the Global Electric Circuit at the Xanthi site. Finally, it is shown that atmospheric CO_2 measurements can be effectively utilized as a stratification proxy, indicating conditions of potential radon trapping, whereas CO_2 was found to anticorrelate with the atmospheric electric field during such conditions.

Keywords: Atmospheric electric field, Potential gradient, Global electric circuit, CO_2

Introduction

The relationship of global atmospheric electric circuit (GEC) with solar–terrestrial interactions (Rycroft et al. 2012) and climatic change monitoring (Rycroft et al. 2000) highlights the significance of conducting atmospheric electricity observations. Nevertheless, a deficit is generally present in qualitative and continuous measurements of atmospheric electricity properties (Israelsson and Tammet 2001), which likely has led to an incomplete knowledge of GEC and its relationship with interacting factors (Dolezalek 1972; Israelsson and Tammet 2001; Reddell et al. 2004).

The most suitable parameters for monitoring GEC are the ionospheric potential, vertical air–earth conduction current, and atmospheric electric field measured at the surface (Rycroft et al. 2008). The latter is known as potential gradient (PG). By convention, PG is defined as the ratio of the local potential at height z to that height, $PG = dV(z)/dz$. PG is defined to be positive during fair weather (FW) days and is related to the vertical component of the atmospheric electric field by $Ez = -PG$. PG

has the capability to reflect changes in GEC if measured at pollution-free sites such as oceans, mountain peaks, and Antarctica and during FW conditions (Reiter 1974; Harrison 2013; Siingh et al. 2013). Moreover, PG is one of the most commonly measured atmospheric electrical parameters for long periods (Nicoll 2012). The resulting abundance of historical and contemporary data for different latitudes helps to improve the understanding of GEC (Märcz and Harrison 2003).

PG observations at continental sites, which are generally not considered ideal for GEC monitoring, are more abundant than those in relatively clean environments. PG at continental sites is subject to influences from local factors such as aerosol pollution, space charge, and natural radioactivity, which are able to alter or mask the daily and seasonal GEC signal (Rycroft et al. 2008). However, these effects do not prevent PG measured under FW conditions from showing features of GEC at some times or through averaging (Harrison 2004a), making that way continental sites also useful in GEC observation. Further, because PG at continental sites is subject to influences from aerosol pollution, space charge, and natural radioactivity, as previously mentioned, its study at such sites may also offer insights into

* Correspondence: nkasteli@env.duth.gr
Department of Environmental Engineering, School of Engineering,
Democritus University of Thrace, 12 Vas. Sofias Str, 67100 Xanthi, Greece

Springer

a variety of other phenomena, processes, or events such as fires (Mather et al. 2007; Ippolitov et al. 2013; Conceição et al. 2015), air pollution (Harrison 2006; Silva et al. 2014), visibility (Harrison 2012), boundary layer monitoring (Piper and Bennett 2012), natural radioactivity assessment (García-Talavera et al. 2001; Latha 2007), and earthquakes (Silva et al. 2011; Silva et al. 2012). Moreover, the usefulness of PG measurements in the research of severe meteorological phenomena such as thunderstorms cannot not be disregarded (Pawar et al. 2014; Pawar et al. 2015).

The use of the Carnegie curve is a typical method for identifying periods in hourly, seasonal, and annual time scales when PG represents global variations or local factors. The Carnegie curve, having resulted from PG measurements of the Carnegie cruise ship conducted at various points on the world's oceans, shows the diurnal variation in PG which is related to global thunderstorm activity and is considered as the global FW background PG (Harrison 2013). A comparison of the standard Carnegie curve with PG measurements at Eskdalemuir, Scotland, has shown that although the station is of continental character and the aerosol periodicity was expected to determine PG variation, the PG closely follows the GEC cycle; this behavior is more pronounced during winter (Harrison 2004a). The same was observed at other Northern Hemisphere continental stations including those in Marsta, Sweden, and Nagycenk, Hungary (Israelsson and Tammet 2001; Märcz and Harrison 2003).

Analysis of atmospheric electricity observations at as many locations around the world as possible is required for a better understanding of the GEC (Kumar et al., 2009). Thus, efforts have been invested in the development of networks (Sheftel et al. 1994; Popov et al. 2008) and databases (Dolezalek 1992; Tammet 2009), which can provide atmospheric electricity data from different locations. The comparison of PG measurements from sites displaced at substantial distances could identify common variations, which are attributed to the global circuit in the absence of coincident local factors (Harrison 2004b). Moreover, PG observations at a variety of global locations could provide an opportunity for better understanding of the local factors controlling PG and, as previously mentioned, for helping to advance our understanding of a variety of geophysical processes.

In this study, 4 years of PG data recorded from February 2011 to December 2014 at a newly established rural station are presented. The data for a 1-year period of June 2011 to May 2012 are analyzed more thoroughly considering ancillary data available for this period. The station is located in the southern Balkans near Xanthi, Greece, and is the only one in this region. The next closest stations are in Nagycenk, Hungary, at a distance of 970 km (Märcz and Harrison 2003) and in Mitzpe Ramon, Israel, at 1500 km (Elhalel et al. 2014). In addition to the presentation of the local PG climatology, the suitability of the site in observing GEC is examined in this study.

Further, the possibility of utilizing atmospheric CO_2 measurements in assessing the daily variation in PG is studied, and special consideration is made for the times at which enhanced stratification coincides with the anticipated occurrences of the GEC signal. Because this is a novel aspect in the studies of PG related to atmospheric gases (e.g., Guo et al. 1996), we plan to address this topic more thoroughly in future work.

Methods
Study site
The study location is a rural site on the Campus of Democritus University of Thrace (41.15° N, 24.92° E, 75 m above sea level) near the town of Xanthi (population 65,000), Greece. The site is at the edge of a smooth, south-facing slope with a valley reaching the seashore about 20 km to the south and the east–west-oriented Rodopi Mountain Range located to the north (Fig. 1). The ground surface around the station is mostly covered with soil and grass; areas covered by concrete and asphalt are significantly fewer in number. To the south, at a distance of 120 m, a light-traffic road oriented east–west with a traffic density of 10 (nighttime) to 150 (rush hours) cars per hour connects the main urban area of Xanthi with nearby villages. The distance between the station and the edge of the urban area is 1.7 km to the west–southwest; that between the station and the edge of the closest village, with a population of 3600, is 0.9 km to the east (Fig. 1). As previously mentioned, the station fills an observational gap in the region because it is the only station within a radius of approximately 1000 km. This station is hereafter referred to as Xanthi station.

The winds blowing at the site exhibit a rather stable diurnal variation possibly owing to the site location at the boundary between a mountainous area and a valley, which triggers a valley/land breeze closed circulation cell. During the night, the prevailing winds blow from the northwest, whereas after sunrise, the wind direction gradually shifts to southwest, south, and southeast before returning to northwest after sunset.

Instrumentation
An electric field meter (EFM; CS110; Campbell Scientific Co., Utah, USA) has been installed since February 2011. The EFM is mounted on a 2-m mast in reversed position and is surrounded by natural and man-made obstacles such as trees, buildings, poles, and cargo containers. However, these obstacles are at a distance of at least 30 m and do not protrude higher than 18° above the
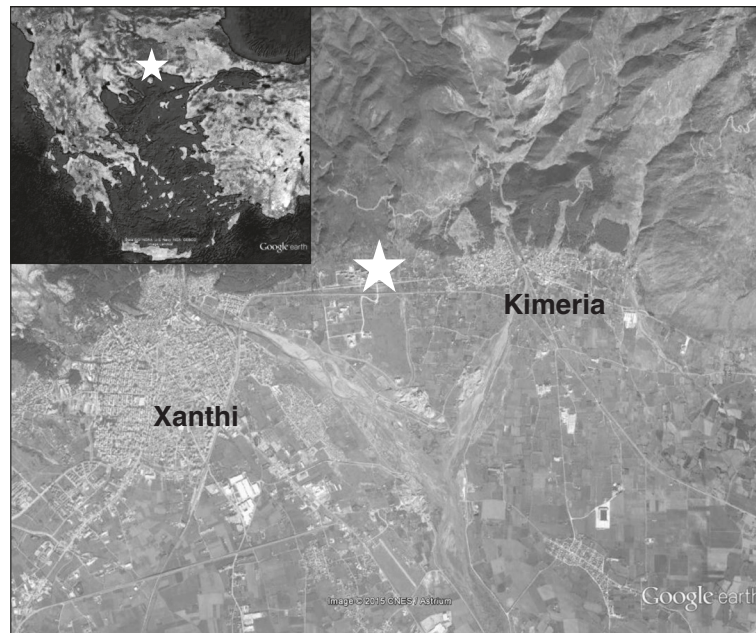
Fig. 1 Map of the Xanthi area, Greece. The station location is denoted by a *star*. The image represents an area approximately 7 km across. *Inset*: the location of the station in the wider area

horizon, as seen from the ground at the EFM location, and hence have minimal effects on the measurements (Campbell Scientific Inc. 2011). Dolezalek (1992), citing Benndorf's calculations, stated that the PG values are representative if the distance between the measuring sensor and any field-distorting disturbance is five times the height of that disturbance or three times the height for thin obstacles such as poles. Our site meets these conditions; other stations have similar site characteristics (Kumar et al. 2009; Piper and Bennett 2012; Smirnov 2014).

Because CS110 is a factory-calibrated field mill, no further calibration is needed for its use (Campbell Scientific Inc. 2011). However, the determination of a site-dependent correction coefficient (C_{site}) is essential because of the EFM's elevated and reversed position, which alters the effective gain with respect to an upward-facing flush-mounted installation (MacGorman and Rust 1998). The coefficient C_{site} was determined statistically (Defer et al. 2015) based on the consideration that FW conditions correspond to the theoretical PG value of 100 V m^{-1} (Takagi and Iwata 1980; Rakov and Uman 2006). C_{site} was calculated by selecting a group of reference FW days and dividing the mean daily PG of each of these days by the typical FW–PG of 100 V m^{-1} to obtain a number of daily C_{site} determinations. Finally, an overall C_{site} correction coefficient was determined as the mean of the 50 % of the daily C_{site} determinations around the median and was used subsequently to correct the PG data. The resultant PG values are considered relative

with respect to the typical FW–PG (100 V m^{-1}) owing to the statistical method used to define C_{site}. The reference FW days were selected from the dataset by using elements from the FW classical definition (Israelsson 1978), i.e., cloud cover less than 3/10 based on the Moderate Resolution Imaging Spectroradiometer (MODIS) satellite MOD08_D3.051 cloud dataset with a resolution of $1° \times 1°$ (King et al. 2003; Remer et al. 2005), wind speed (WS) less than 3 on the Beaufort scale (4 m s^{-1}), no precipitation events, and the 1965 definition of the International Commission on Atmospheric Electricity (Israelsson 1978). On the basis of the latter, days having at least one mean hour PG < 0 V m^{-1} were considered as disturbed weather (DW) days; negative PG values were attributed to local generators and were excluded. The resulting days span the entire period, hence eliminating any possible seasonal bias.

The EFM operated under two resolution modes because measurements were conducted under all weather (AW) conditions including both FW and DW. For measurements falling within the range 0–2.2 kV m^{-1}, the resolution was 0.32 V m^{-1} and for those falling within 2.2–22.3 kV m^{-1} was 3.2 V m^{-1}.

Measurements of atmospheric CO_2 by using an instrument equipped with a Gascard II Edinburgh Sensor (Schumann Analytics, Germany) were conducted along with PG within the period June 2011 to May 2012, covering 150 days throughout the seasons. The CO_2 analyzer was calibrated against a reference analyzer.

Ambient air was continuously sampled from the exact point at which the PG was measured, 2 m in height, by using a pump at a rate of 0.52 l s^{-1}.

Standard meteorological parameters such as WS/direction, temperature, relative humidity, pressure, and precipitation were also recorded since June 2011 by using commercially available sensors that were located at the same site as that of the EFM. WS and direction were measured by using a Wind Sentry Set (Model 03002L; Young Co., Michigan, USA) consisting of a three-cup anemometer and a wind vane with accuracies of ±0.5 m s^{-1} and ±5°, respectively. Temperature and relative humidity were measured by using a thermometer/hygrometer of ±1.5 % and ±0.3-K accuracy (Model HygroClip S3; Rotronic Co., Switzerland). The pressure was measured by using a barometric pressure sensor of 0.3-hPa accuracy (Model PTB110; Vaisala Co., Finland). The precipitation was measured by using a tipping bucket rain gauge (Model 52202; Young Co., Michigan, USA). Two extra temperature (T) sensors (HOBO Pro v2 T/RH U23-001; Onset, Massachusetts, USA), with solar shields at ±2 % accuracy and ±0.02 % precision, were deployed from February 2012 to May 2012 at heights of 2.5 and 1.5 m to provide the vertical temperature gradient (DT).

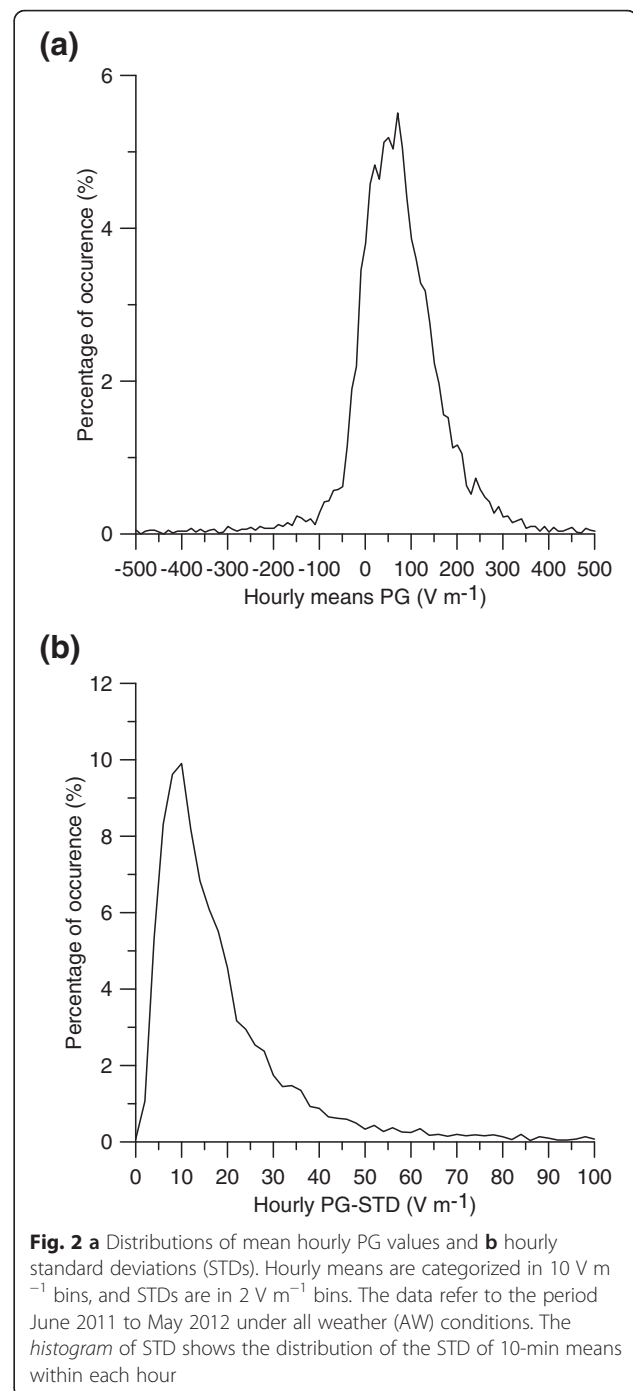All sensors operated at a frequency of 1 Hz with the exception of the extra T sensors at $f = 1/60$ Hz, and the data were recorded as 1-min means. One-minute PG data were subsequently used to calculate 10-min data, which in turn were used to calculate the hourly means. The PC used for data acquisition was synchronized at regular intervals to the National Institute of Standards and Technology (NIST) time server. Local time (LT), wherever used in the manuscript, refers to Coordinated Universal Time (UTC) + 2; hence, no Daylight Saving Time was applied in summer.

The presented data cover the period February 2011 to December 2014. Data from the period June 2011 to May 2012 were analyzed more thoroughly. Thus far, that period is the only full year with continuous PG measurements and data for all of the other variables.

Results and discussion
PG observations and FW set selection
In Fig. 2, the histogram of the hourly PG means is presented in 10 V m^{-1} bins for the period June 2011 to May 2012 under AW conditions. The vast majority of the values (93.6 %) was concentrated in the range of −200 to 350 V m^{-1} with all bins presenting a >0.1 % frequency of occurrence. The mean value and standard deviation (STD) were 66.24 and 649.90 V m^{-1}, respectively. This STD is exceptionally high owing to the occurrence of DW conditions, e.g., thunderstorms, which could cause PG values up to 15 kV m^{-1} or even

Fig. 2 a Distributions of mean hourly PG values and **b** hourly standard deviations (STDs). Hourly means are categorized in 10 V m^{-1} bins, and STDs are in 2 V m^{-1} bins. The data refer to the period June 2011 to May 2012 under all weather (AW) conditions. The *histogram* of STD shows the distribution of the STD of 10-min means within each hour

greater (MacGorman and Rust 1998), while the site exhibits some of the highest keraunic levels reported in the southern Balkan Peninsula (Mazarakis et al. 2008; Chronis 2012). We note here that the keraunic level is defined as the average number of days per year when thunder can be heard in a given area and presents the likelihood of a thunderstorm occurrence. DW conditions are not confined to thunderstorms but also include cases of charged clouds' region passage over the EFM and rain

showers. These factors are considered to cause PG values that extend beyond the range of $-200 \text{ V m}^{-1} < \text{PG} < 350 \text{ V m}^{-1}$ because of their strong electrostatic nature, constituting the remaining 6.4 % of the total distribution.

A significant element of the distribution is the amount of hourly values falling into the range $-200 < \text{PG} < 0 \text{ V m}^{-1}$, which constitutes 16.9 % of the dataset, in contrast with that at other sites, where negative values are much less frequent (Bennett and Harrison 2007; Israelsson and Tammet, 2001). These hours can be attributed to DW conditions because they commonly cause PG reversal to negative values. The majority of these values occur during the night, regardless of weather conditions; that implies the existence of a local generator (local source of space charge generation) sufficiently strong for producing sufficient negative space charge for PG reversal (Piper and Bennett 2012). Because of the timing and the repeatability of the phenomenon, the most probable generator is natural radioactivity. Under nocturnal inversion, radioactive substances such as radon and its daughter products are trapped close to the ground, causing the reversed electrode effect and increasing negative space change density, which subsequently reduces PG (Hoppel et al. 1986). The assumption that natural radioactivity is a local generator that causes PG reversal is further supported by the fact that the station site overlies granitic deposits and uranium ores (Pergamalis et al. 1998; Pergamalis et al. 2010) and exhibits some of the highest radon fluxes in Europe. This factor, which has been confirmed by models (López-Coto et al. 2013) and recent observations (Kourtidis et al. 2015), could be also responsible for increased conductivity close to the ground (Latha 2007). Along with the generally low aerosol concentrations that our site exhibits, as a typical rural site away from heavy pollution sources like industries and major cities such as Athens (Retalis and Retalis 1997), this factor was responsible for a reduced AW mean value of 66.24 V m^{-1} (Israelsson and Tammet 2001).

For the same period, a histogram of hourly STD calculated from 10-min means is also presented in Fig. 2. The distribution shows a pronounced positive skew denoting relative sub-hourly stability. The greatest percentage of hourly means, 91 %, exhibits STD < 100 V m^{-1}, implying that most hours comply with the FW conditions criteria (Harrison 2011). Despite the relative sub-hourly stability, the PG still shows small fluctuations within each hour mostly between 4 and 20 V m^{-1}, reflecting the effects of changing local factors such as space charge and aerosols.

Thus far, it is evident that both hourly PG values and their respective STDs are strongly influenced by the prevailing meteorological conditions during that hour (i.e., existence of thunderstorms, charge clouds passage) and the existence of local generators (e.g., radon). These influences are of local origin and are capable of completely masking the response of PG to GEC diurnal variation. To permit examination of the diurnal and seasonal variation of PG without the interference of DW conditions and those with intense ionization, an FW–PG dataset was created. Two simple criteria were used to determine the data to be included in the FW set: $0 < \text{PG} < 350 \text{ V m}^{-1}$ and PG-STD < 100 V m^{-1}. Negative PG values were excluded because they are attributed either to local generators (natural radioactivity) or to DW conditions. Moreover, those of more than 350 V m^{-1}, or ~2.7 % of the distribution, were excluded because they are attributed to DW conditions or high aerosol concentration events. The extra filter of PG-STD > 100 V m^{-1} was applied to eliminate any hourly values that eventually fell within the range of 0–350 V m^{-1} through the averaging process, although they were recorded during DW conditions. The FW set was composed of 78 % of the total number of hourly means of the examined period. We note here that this high percentage of FW hours is favorable for the station compared with that at stations farther northward in Europe.

The method of using PG statistics as a means to identify the conditions under which it was measured and to eventually define an FW–PG set is useful, particularly for cases in which cloud cover and local generators activity data are not available in high resolution and thus the classical FW definition can be utilized (Israelsson 1978). Such is the case for the Xanthi site. Applications of that method are found for Marsta Observatory (Israelsson and Tammet 2001), Nagycenk Geophysical Observatory (Märcz and Harrison 2003), and elsewhere (O'Connor 1976; Burns et al. 2005) with criteria customized for each site.

Diurnal and seasonal PG variation

The diurnal variation of FW–PG exhibits two characteristic patterns, those of single and double peaks (Chalmers 1967). The single peak (Carnegie curve) is followed at environments in which local effects (e.g., pollution) are low or absent like oceanic (Harrison 2013), polar (Siingh et al. 2013), mountaintops [e.g., Wank peak (Reiter 1974)], and remote isolated sites [e.g., Eskdalemuir (Harrison 2003; Harrison 2004a)] depicting the global thunderstorm activity. Moreover, a single peak is exhibited at certain stations during wintertime, particularly at high latitudes (Israelsson and Tammet 2001; Harrison 2004b), showing high correlations with the Carnegie curve. The double peak is followed at continental stations (Retalis and Retalis 1997; Harrison and Aplin 2002) and is generally synchronized with local time and the intensity of local effects (Chalmers 1967), while the GEC signal is not always apparent and

averaging over one or several weeks is needed to be shown (Dolezalek 1972).

The mean diurnal variation of FW–PG in Xanthi exhibited the typical continental course, that of the double peak (Fig. 3). The primary maximum was evident between 11:00 and 12:00 LT, and the secondary maximum occurred at 21:00 LT; the corresponding preceding minima appeared at 5:00 and 18:00 LT, respectively.

The increasing trend of FW–PG during the morning hours and the following primary maximum around noon is attributed to local factors, namely "sunrise effect" and aerosols.

The sunrise effect was extensively described by Marshall et al. (1999), who focused particularly on PG response to positive space charge transpositions. Other authors (Law 1963; Chalmers 1967; Kamra 1982) also mentioned the sunrise effect, among which Kamra (1982) and Law (1963) observed a sign reversal of space charge from negative to positive at the moment of sunrise, coinciding with PG increase. According to Marshall et al. (1999), the start of the morning convection caused by solar heating leads to the destruction of a shallow positively charged layer (electrode layer) that was built up during the night and overlies the very first decimeters of the ground (Crozier 1963). The dilution of the electrode layer just after sunrise owing to increasing turbulence transports gradually more and more positive charges over the EFM enhancing eventually PG (Marshall et al. 1999). The mechanism weakens as time passes and the boundary layer becomes well mixed (Moore et al. 1962). The PG increase attributed to the sunrise effect might be further intensified at our site because of the location of the station downslope of a mountainous area and the possibility of valley or land breeze closed circulation cells. In that case, the electrode layer that was formed on the mountain's surface during the night is also diluted after sunrise, and after being transported upslope, the positive charges can be advected over the EFM via the returning cell circulation. The significance of the sunrise effect on the morning peak was also emphasized in studies for other stations, irrespective of the character of the site, including typical continental (Retalis and Retalis 1997), tropical continental (Latha 2003), or island tropical (Kumar et al. 2009).

Aerosols have a direct impact on local conductivity by acting as recombination centers for the ions; at the same time, aerosols reduce the mobility of the ions attached to them, thus reducing further conductivity (Hoppel et al. 1986; Harrison and Carslaw 2003). A decrease in local conductivity, considering a steady conduction current between the ionosphere and the ground, provokes a PG increase in accordance to Ohm's law (Jayaratne and Verma 2004). Aerosols in our site are expected to have increased arithmetic concentration at the ground level during the morning to noon hours, thus increasing PG. The increased aerosol levels are attributed to enhanced road traffic south of the station. The effect of aerosols on PG is further enhanced because of the direction of the wind typically blowing southeast to southwest at that time, which transfers more aerosols toward the EFM instrument. Hence, at our station, it is possible that the southern winds and the upwind road traffic, both of which are more intense after 9:00–10:00 LT, resulted in greater aerosol concentration around the station and followed the sunrise effect. This process may have provoked a continuous increasing effect on PG, which eventually maximized at 11:00–12:00 LT.

An extra factor that can contribute to the morning increasing trend of PG is thunderstorm activity in Asia, which was at its maximum at that time (Harrison 2013; Blakeslee et al. 2014). The contribution of that parameter is considered rather low compared with the aforementioned factors, yet it is mentioned here as the only global factor that may act on the local primary PG maximum.

After the primary maximum, PG subsided and eventually reached a minimum at 18:00 LT. This is attributed to the maximization of convective conditions in the late afternoon, which can cause aerosol depletion close to the ground by dilution. Aerosols are transported upward, allowing ion concentrations to recover. Thus, local conductivity is increased and PG is subsequently reduced (Chalmers 1967; O'Connor 1976; Serrano et al. 2006; Silva et al. 2014), in accordance with Ohm's law under constant air–earth conduction current of $PG = J_Z/\sigma_T$, where J_Z is the air–earth conduction current, and σ_T is total conductivity (Harrison 2006). Upward transport of aerosols gradually provides an extra suppression to PG through a decrease in the conduction current. Because there is no mechanism for quickly removing aerosols

Fig. 3 Mean diurnal variation of fair weather (FW)–potential gradient (PG) and all weather (AW)–PG for the period of June 2011 to May 2012. *Error bars* denote standard errors for each hour. *Upward* and *downward arrows* denote mean sunrise and sunset time, respectively
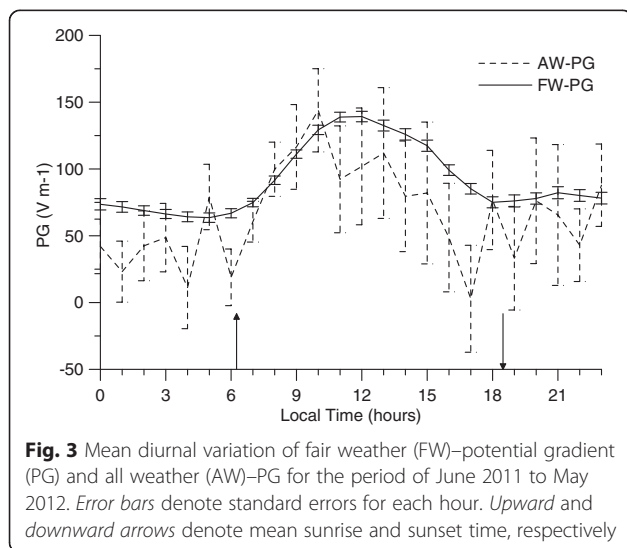
while they are elevated, an increase in columnar resistance results, reducing the air–earth conduction current (generating force of PG) and subsequently reducing PG (Harrison and Bennett 2007). Considering the moment of PG minimum at our site at 18:00 LT, a delay in columnar resistance maximization was noted in comparison with the results of Sagalyn and Faucher (1956), where the corresponding maximum occurred at 15:00 LT. We tentatively attribute this delay to differences in advective conditions at each site. In particular, the Sagalyn and Faucher (1956) maximum columnar resistance was obtained during low advection periods, whereas at our site, advection was expected to be relatively high because of the station's location and thus change the columnar aerosol load.

The secondary maximum occurring at 21:00 LT and the following minimum at 05:00 LT coincide with the corresponding Carnegie curve extrema at 19:00 and 03:00 UTC, depicting the diurnal variation of global thunderstorm activity. However, both extrema are susceptible to local effects that could enhance or suppress the global signal. The convective conditions maximized earlier that caused a minimum at 18:00 LT were gradually weakened, resulting in increased aerosol concentration close to the ground and subsequently increased PG, as described above (Latha 2003). On the contrary, the gradual transition to nocturnal stratification could cause trapping of radon and its progeny, resulting in intense ionization conditions and the creation of negative space charge (reversed electrode effect), which would eventually suppress PG (Hoppel et al. 1986; Latha 2007). Negative space charge can also reverse PG polarity; however, negative values were not considered here because FW–PG is the focus. The effect of radon under nocturnal inversion can also affect the PG minimum (05:00 LT) on certain days. The magnitude and the specific timing of the effects of local factors on the global signal of PG are not easily defined; therefore, measurements of additional variables such as aerosol soundings, ground aerosols, conductivity, and radon are needed.

A comparison of the magnitude of the primary peak with the magnitude of that coinciding with the Carnegie peak revealed an obvious substantial difference such that local effects are dominant at Xanthi during the day much more than the global effects. The diurnal variation of AW–PG (Fig. 3) follows the same course as that of FW–PG, and for the greatest part of the day, it is kept below the FW curve; this coincides with PG behavior at other sites (O'Connor 1976; Retalis and Retalis 1997). As is apparent from its unstable daily cycle, AW–PG experiences greater fluctuations than FW–PG; this result was expected because DW conditions were included. Strong hourly variability was also evident from the enhanced standard errors (SE), where SE = STD/$\sqrt{n}$. Although n is

not the same for all hours, it is sufficiently high to assure comparable SEs. The enhanced SE showed a pronounced intensity between 11:00 and 21:00 LT. During the same period, lightning activity is increased over Greece (Chronis 2012) and Xanthi, the latter exhibiting the highest keraunic levels in the country (Mazarakis et al. 2008). Lightning activity is maximized between 16:00 and 17:00 LT (Chronis 2012), coinciding with the highest difference of the two curves, which in turn indicates a significant existence of non-FW conditions in the AW set during these hours (O'Connor 1976). Similar differences between the two curves were also apparent during certain night hours, although the non-FW conditions here are more likely attributed to natural radioactivity. Consequently, although the AW–PG generally followed a typical double-peak diurnal oscillation, the DW conditions at our site were sufficiently intense and occurred often, thus causing the minima and maxima of the curve to be significantly fuzzier than those of FW–PG.

All months followed the general pattern described above, although in some cases, both extrema were not apparent (Fig. 4). During the warm months of June to October, the PG exhibited its primary maxima at 10:00–11:00 LT, whereas during the cold months of November to January, the corresponding maxima were transposed to 12:00–14:00 LT. This transposition is attributed to the earlier initiation of convective conditions during the warm months and the subsequent earlier activation of the sunrise effect (Latha 2003) and is in agreement with the results at other continental sites (Retalis and Retalis 1997). The remainder of the months, February to May, showed intermediate behavior, exhibiting their maxima at 11:00–12:00 LT. The secondary maximum is not clear in every month, denoting the influence of local factors on PG at the time of global thunderstorm maximization. However, when a secondary maximum was apparent in August, September, January, and May, it occurred within ±1 h from the Carnegie curve maximum of 19:00 UTC. The timing difference could be attributed to seasonality of local factors such as aerosols, regional changes in the thunderstorm distribution, which could disturb the typical GEC cycle (Harrison 2004a), or ionospheric perturbations (Harrison 2004b). Finally, the two minima did not show seasonality and were centered at 05:00 and 18:00 LT, respectively. Because the months showing the secondary peak span the entire year, this effect is not solely seasonal. It could be hypothesized that it is the outcome of a combination of more than one influencing factors such as radon emanation, turbulence, and aerosol concentration and size distribution. However, in the absence of relevant data, such assumptions can only be speculative.

The seasonal variation of FW–PG observed during the period February 2011 to December 2014, with maxima
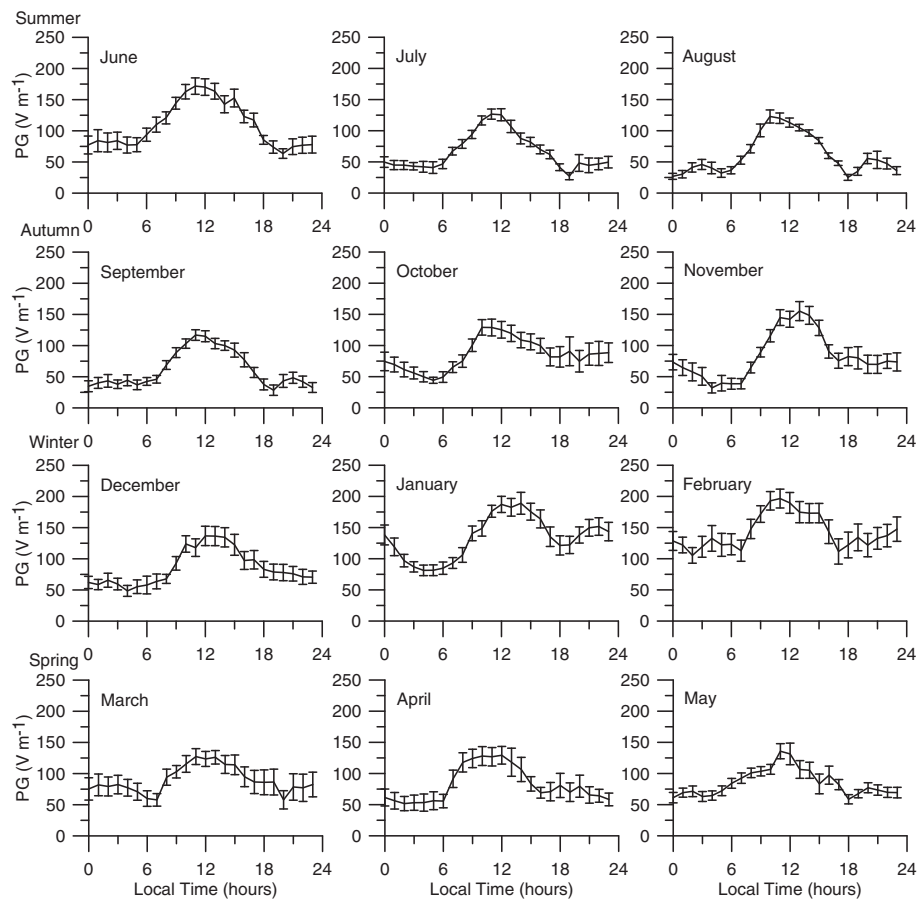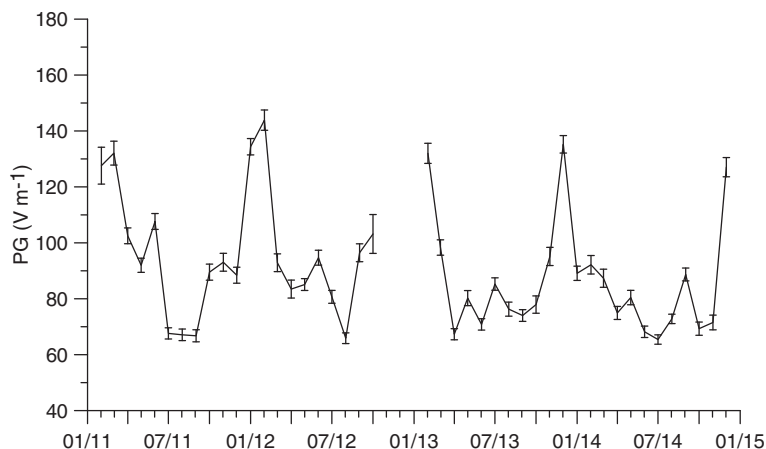
Fig. 4 Mean diurnal variation of fair weather (FW)–potential gradient (PG) for each month of the period June 2011 to May 2012. Months are aligned per season. *Error bars* denote the standard error

(minima) during cold (warm) months (Fig. 5), is in agreement with the results at other continental sites of the Northern Hemisphere (Chalmers 1967; Israelsson and Tammet 2001; Bennett and Harrison 2007a). Concentrations of Aitkin nuclei near the ground, which act as the ultimate sink for small ions close to the ground, are maximized during the cold months owing to the reduced vertical mixing of the atmosphere (Adlerman and Williams 1996 and references therein). During the cold months, heating increases aerosols in settlements. However, that fact is insufficient for explaining the increased aerosol concentrations close to the ground in winter because the main heating sources in the vicinity, including the town of Xanthi and the village of Kimeria, are not upwind of the dominant wind directions encountered at the site. Additionally, in Greece, columnar aerosol concentrations usually peak in spring/summer; from a source intensity perspective, additional sources exist in summer also. From an atmospheric pollution perspective, the boundary layer height (BLH) is the main driver of the aerosol concentrations close to the ground. This occurs because at Mediterranean sites at the same

latitude as our site, the BLH during summertime can be at times even 10 times greater than that during winter owing to the decreased convection during winter (e.g., Georgoulias et al. 2009). The large amounts of Aitkin nuclei very effectively reduce the concentration of small ions that dominate the electrical conductivity of air, which leads to reduced local conductivity and subsequently to PG maximization. The opposite occurs during the warm months, when the boundary layer is substantially deeper than that in winter and thus scavenges aerosols that are close to the ground. The aforementioned mechanism is also in agreement with earlier measurements of atmospheric ions conducted in Athens (Retalis 1983; Retalis et al. 2009). These measurements have shown maximum (minimum) small ion concentrations during summer (winter). On the contrary, large ions that are positively correlated with pollution and act as a complementary sink for small ions followed the opposite trend: that of PG (Retalis and Retalis 1997).

Consequently, the long-term FW–PG variation at our site, which is a typical continental site in the Northern Hemisphere, is attributed to the seasonality of ground

Fig. 5 Long-term variation of fair weather (FW)–potential gradient (PG) for the period February 2011 to December 2014. Mean monthly values were calculated from hourly means. *Error bars* denote the standard error

aerosol concentration. Variability in extrema timing and fluctuations during the months between the maximum and the minimum may be attributed to factors influencing the aerosol concentration such as vertical mixing and to probable global lightning activity changes.

Local versus global effects

Observing GEC from a single continental station is a challenging task because, as previously mentioned, local effects such as aerosols and space charge can completely mask the global variations (Rycroft et al. 2008). However, local effects are either minimized during certain periods or they do not change considerably in time, permitting the observation of global signals (Harrison 2004b). An attempt to identify such periods for our site is presented here by comparing FW–PG with the Carnegie curve (Rycroft et al. 2008).

The GEC does not follow always a typical Carnegie curve owing to conditions such as lightning activity variations and ionospheric perturbation; therefore, strict conclusions resulting from any type of comparison with the Carnegie curve should be avoided (Harrison 2004b). However, the Carnegie curve is widely accepted as a basic tool for identifying the periods in which PG reflects GEC variation as long as the PG data are averaged over a suitably long period (Rycroft et al. 2008). That is the case in the current manuscript. Additionally, although Harrison (2013) reported a marginal latitudinal dependence of PG, the latitude effect influences the absolute PG values. The comparison of local PG versus the Carnegie curve was made in the present study through the corresponding percentages of the means. As a result, such influences were eliminated. The FW–PG follows a parallel course to global variation, whereby its minimum at 03:00 UTC and secondary maximum at 19:00 UTC coincide with the Carnegie curve extrema; however, a

disruption was evident during the evolution of the primary maximum at 04:00–16:00 UTC (Fig. 6). When estimating the differences between the two cycles (DPG = FW–PG, Xanthi as percentage of mean – the PG Carnegie curve as percentage of mean) the greatest deviation from the Carnegie curve occurs between 8:00 and 12:00 UTC, with a maximum difference of 58 % at 9:00 UTC. This is attributed to the sunrise effect and aerosols, as previously discussed. During 14:00–16:00 UTC, the PG at our site became lower than the Carnegie curve, creating a negative DPG. This subsidence can be attributed to the maximization of the convective conditions, which caused an increase in the aerosol columnar load and a subsequent decrease in the conduction current and PG in accordance with Ohm's law (Serrano et al. 2006). DPG remained negative during 16:00–4:00 UTC, the
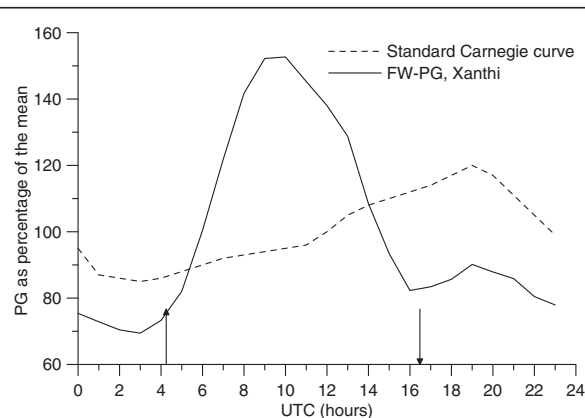
Fig. 6 Mean diurnal variation of Xanthi fair weather (FW)–potential gradient (PG) for June 2011 to May 2012 and the standard Carnegie curve. Each curve is presented as a percentage of its mean. Data of the standard Carnegie curve (cruises IV, V, and VI) were acquired from Table II of Harrison (2004c). *Upward* and *downward arrows* denote mean sunrise and sunset time, respectively

time at which the PG followed the same trend as the Carnegie curve ($r = 0.98$, $p < 0.01$), yet gradually reduced in magnitude throughout the night. The gradual suppression of the boundary layer and the resulting stratification of the atmosphere, which followed the peak of convective conditions, may have increasingly enhanced radon trapping (Latha 2007). The latter could cause an increase in negative space charge over the EFM, thus reducing the PG (Israelsson and Tammet 2001). As the transition to nocturnal stability was completed, the variability of factors that could cause large fluctuations in PG, such as aerosols and radon, was reduced, allowing the PG to follow the Carnegie variation closely. DPG between 21:00 and 04:00 UTC fell below 25 %; that at 01:00–04:00 UTC fell below 15 %, which were considered to be the most preferable hours during the day for GEC observations at our site. The same hours (01:00–04:00 UTC) were also considered to favorably represent the GEC observations at the Nagycenk Geophysical Observatory continental station in Hungary (Märcz and Harrison 2003).

To determine which months deviated less from the Carnegie curve and thus are more suitable for GEC observation, the DPGs between the two diurnal variations were calculated again for each month of the period June 2011 to May 2012 (Fig. 7). Cold months of October–March excluding November exhibited low to moderate deviations from the Carnegie curve during the entire day, whereas the warm months of April–September showed large differences that were not confined to the moments of primary maximum but also occurred during afternoon and early evening (Fig. 7). Such a trend is again associated with atmospheric convection, which is more intense during the warm months. During the cold

Fig. 7 Difference between fair weather (FW)–potential gradient (PG) at Xanthi and the standard Carnegie curve (DPG). The DPG is presented as a percentage of the difference from the mean during different months and the time of the day for the period June 2011 to May 2012

months, the atmosphere is more stable, resulting in lower diurnal variations in aerosol and radon concentrations. This means that the variability of the columnar resistance and local conductivity are also reduced; thus, ionospheric changes caused by global thunderstorm activity can be shown in a PG diurnal pattern. Cold months are also preferable in GEC observations at other continental sites (Israelsson and Tammet 2001; Märcz and Harrison 2003; Harrison 2004a; Harrison 2004b; Serrano et al. 2006), in which the responsible mechanism is again considered to be atmospheric convection seasonality. November's deviation from the general pattern of cold months during the largest part of the day could be attributed to intensified atmospheric mixing or temporary enhancement of local factors such as aerosols and space charge.
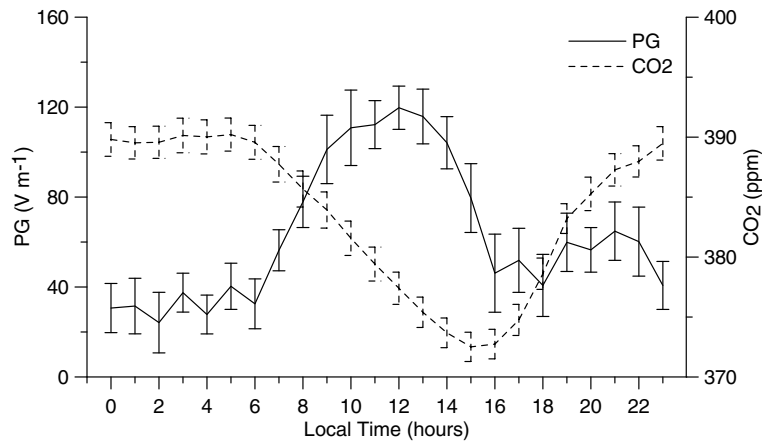
PG and atmospheric CO_2

The significance of micrometeorology in atmospheric electricity has long been established (Israelsson and Oluwafemi 1975), and studies have been performed on correlating micrometeorological elements with PG (Law 1963; Barlow and Harrison 1999; Latha 2007). Here, the use of atmospheric CO_2 as a stratification indicator in the assessment of PG is discussed. Although CO_2 and PG are two variables of completely different natures, they are both affected by convective conditions; thus, a common element is utilized for interpretation of the PG diurnal cycle.

In Fig. 8, the mean diurnal variation of common PG and CO_2 values is presented for the period June 2011 to May 2012. The PG values used here were obtained from the AW dataset, excluding the days with rain and days when $|PG| > 1$ kV m^{-1}, the latter denoting the existence of heavily charged clouds (Bennett and Harrison 2007b). The aforementioned values were excluded because they refer to disturbed conditions that dominate PG variation with no impact on CO_2. A comparison of the two cycles revealed a reverse relationship between PG and CO_2 ($r^2 = 0.36$, p value <0.01) despite the variability of non-common driving factors such as aerosols, space charge, GEC, photosynthesis, and transpiration during the day (Fig. 8).

During the night, at 21:00–06:00 LT, stratification in the atmosphere confined the vertical mixing, thus allowing radon trapping, which eventually caused PG reduction by favoring negative space charge formation (Latha 2007), while CO_2 concentrations attained their maximum owing to respiration and lack of photosynthesis. After 6:00 LT, the initiation of morning mixing conditions diluted the space charges and photosynthesis began, thus increasing PG and reducing the CO_2 concentration. Between 12:00 and 16:00 LT, both curves followed a parallel downward trend as the vertical
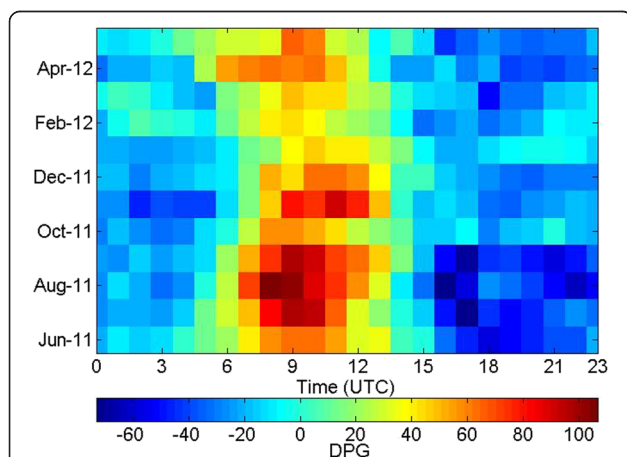
Fig. 8 Mean diurnal variation of potential gradient (PG) and atmospheric CO_2 for the period June 2011 to May 2012. The PG values were obtained from the all weather (AW) conditions dataset excluding the days of precipitation events or $|PG| > 1$ kV m^{-1}. *Error bars* denote the standard error

convection gradually maximized, further diluting the CO_2 and reducing the PG through an increase in columnar resistance and a subsequent decrease in the air–earth current. The latter mechanism referring to PG continued until 18:00 LT. During 16:00–21:00 LT, the CO_2 increased owing to the gradual transition to nocturnal stratification and the enforcement of CO_2 sources such as transpiration. The PG exhibits its secondary minimum at 18:00 LT and then increased parallel to the CO_2 trend, presenting the global thunderstorm activity.

Late afternoon and early night hours, 18:00–00:00 LT, were of special interest. The peak of the global signal was expected at that time, and the concurrent evolution of stratification could have altered or completely masked the planetary effect through radon trapping.

As a case study, PG, CO_2, DT (DT = $T_{2.5m} - T_{1.5m}$), and WS in a 1-min time series were examined for May 1–3, 2012 (Fig. 9). It must be noted that during those days, cloud cover was <1/10 and the WS was <5 and <4 m s^{-1} in most cases, which reduced the possibility of an impact on PG–CO_2 comparison by non-common factors such as charged clouds and blown dust.

When describing the electrode effect, Law (1963) explained that under the influence of FW–PG, positive ions are driven toward the ground and negative ions are repelled from the ground, which creates a deficit of negative ions and the formation of a positively charged layer close to the ground (electrode layer). Under non-turbulent conditions, such as those typically prevailing during nighttime, the electrode layer is suppressed to depths at an order of magnitude of a few decimeters (Crozier 1963). In cases of intense ionization, such as those of high radon concentration caused by trapping under nocturnal stratification, the produced negative charges flee away from ground level and ascend over the shallow electrode layer, thus reversing the electrode effect and forming negative space charge (reversed electrode layer), which subsequently reduces PG (Latha 2007).

Near-ground CO_2 and radon are both strongly affected by atmospheric mixing. Thus, using CO_2 as an indicator of radon trapping and therefore PG variability under nighttime non-turbulent conditions is a reasonable assumption. Law (1963) observed that negative space charge produced from natural radioactivity during night is closely related to the temperature gradient and increases with increasing stability, which in turn increases the CO_2 concentration.

PG and CO_2 were inversely correlated during nighttime during all 3 days (Fig. 9). This may be attributed to the reversed electrode layer formed (diluted) under strong (weak) stratification and the corresponding radon and CO_2 increase (decrease). Minor deviations from that reverse relationship are expected to occur mostly because of aerosol or space charge advection influencing PG. We note here that although stable nighttime conditions can generate a reverse electrode effect, thus obscuring the GEC signal, the 01:00–04:00 UTC period still appears to be the best period to observe the GEC signal at the site (Fig. 7). This could be attributed to the reverse electrode effect reaching the steady state by 01 UTC (03 LT), therefore adding a constant offset to PG and allowing the DPG to subsequently minimize.

The PG global oscillation anticipated between 18:00 and 00:00 LT was not apparent every day (Fig. 9). On May 1, PG showed part of the GEC variation only when calm wind conditions were disturbed (WS > 0.5 m^{-1}), which interrupted the relatively strong stratification (DT > 0.5 °C) while simultaneously reducing the CO_2. Following that short period, calm wind conditions returned, causing enhanced stability (DT increases)
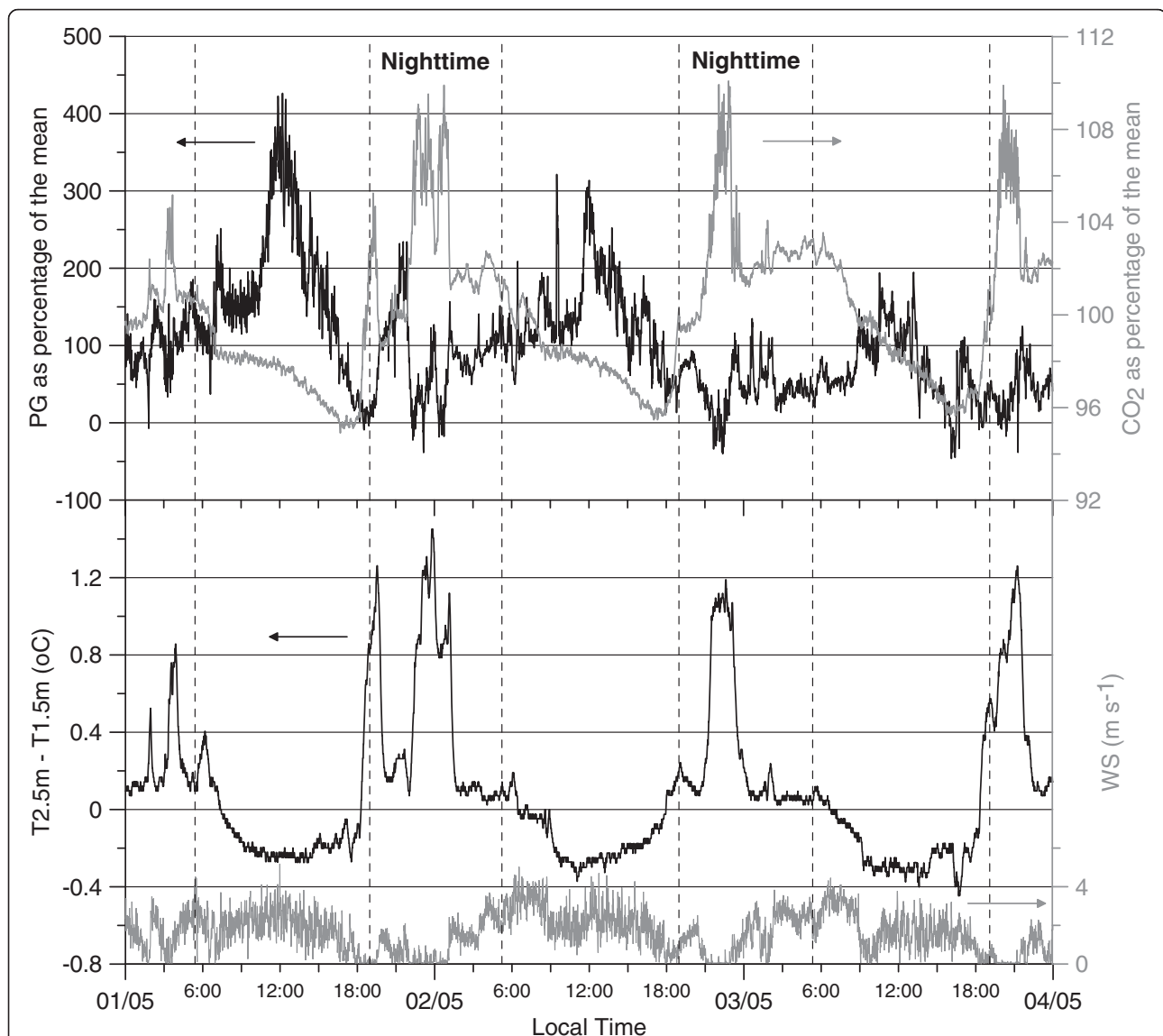
Fig. 9 Observations of potential gradient (PG), CO_2, wind speed (WS), and vertical temperature gradient (DT = $T_{2.5m} - T_{1.5m}$) during May 1–3, 2012. Data are presented at 1-min resolution. PG and CO_2 are presented as percentages of the respective 3-day mean. *Vertical dashed lines* denote sunrise and sunset

which caused the CO_2 to increase and the PG to decrease. The following night, May 2, the stability evolved with no strong disruptions until the GEC peak time at 21:00 LT, except for a short period just after sunset when the stratification slightly weakened. During that short period, the PG increased smoothly, responding to the GEC oscillation, whereas the CO_2 increased rate was temporarily reduced. After that period, the CO_2 continued to sharply increase and reached maximum, whereas the PG decreased significantly, reversing the polarity, and did not show the global signal. During the last night, May 3, nocturnal stratification was initiated and evolved undisturbed, causing a monotonical increase in CO_2 and

completely masking the GEC. The PG remained low and at times reached negative levels.

The evolution of PG and CO_2 during those nights, particularly when the GEC signal was anticipated, suggests that when CO_2 is increasing stably and has high concentrations, PG is suppressed and GEC observation is not possible. Therefore, CO_2 variations during stable nights could be complementarily used for categorizing days as suitable or not suitable in GEC monitoring, assuming the absence of factors that could exclusively change PG such as charged clouds overhead and aerosols. Additionally, single-point CO_2 measurements can be utilized as turbulence proxies and can give information on the evolution of atmospheric electricity

properties (i.e., PG). In that way, a connection between micrometeorology, atmospheric gases, and atmospheric electricity is established.

Conclusions

In this study, the first 4 years of PG observations are presented from February 2011 to December 2014 from a newly established rural station in Xanthi, Greece.

The seasonal FW–PG variation is typical for a continental Northern Hemisphere station, with maxima (minima) during cold (warm) months.

The mean diurnal variation of FW–PG follows a typical double peak of continental sites with the primary maximum between 11:00 and 12:00 LT and the secondary maximum at 21:00 LT. The dominant peak was attributed completely to local factors and specifically to the sunrise effect and the increase of aerosol arithmetic concentration, the latter originating from the initiation of anthropogenic activity. An enforcement of the sunrise effect is probable for the Xanthi site because the station is located at the foot of a hill, and local circulation effects occur after sunrise. The secondary peak could be attributed to global factors because its time of occurrence coincides with the Carnegie curve maximum. However, it is also susceptible to local effects because at the same time, the transition from the maximization of convective conditions to nocturnal stratification could provoke an increase in aerosol concentration (trapped radon) acting positively (negatively) on FW–PG. During warm months of June to October, FW–PG exhibited its primary maxima at 10:00–11:00 LT, whereas during the cold months of November to January, the corresponding maxima were transposed to 12:00–14:00 LT. The remainder of the months, February to May, exhibited an intermediate behavior with maxima at 11:00–12:00 LT. The secondary maximum was apparent only during August, September, January, and May and occurred within 1 h of the Carnegie curve maximum at 19:00 UTC. The diurnal variation of AW–PG generally followed that of FW–PG, although the AW–PG levels were mostly lower. The extensive thunderstorm activity at the site resulted in a deviation of the AW–PG curve from that of FW–PG as well as high AW–PG hourly variability.

The Xanthi nocturnal FW–PG curve correlated strongly with the standard Carnegie curve. The most preferable hours for GEC observation at the Xanthi site were between 01:00 and 04:00 UTC, and cold months favored global signatures more than warm months.

Finally, it was shown that collocated atmospheric CO_2 measurements can be effectively used as stratification proxies to identify conditions that favor radon trapping and subsequently alter PG. Under stable nighttime conditions, when CO_2 increased stably and had high concentrations, PG was suppressed and GEC observation was not possible. Such a reverse relationship of PG and CO_2 during the global signal occurrence could complement the categorization of days as suitable or not suitable in GEC monitoring.

References
Adlerman EJ, Williams ER (1996) Seasonal variation of the global electrical circuit. J Geophys Res 101:29679–29688. doi:10.1029/96JD01547

Barlow JF, Harrison RG (1999) In: Christian HG (ed) Turbulent transfer of space charge in the atmospheric surface layer. Proceedings of the 11th International Conference on Atmospheric Electricity, Guntersville

Bennett AJ, Harrison RG (2007a) Variability in surface atmospheric electric field measurements. J Phys Conf Ser 142:012046. doi:10.1088/1742-6596/142/1/012046

Bennett AJ, Harrison RG (2007b) Atmospheric electricity in different weather conditions. Weather 62:277–283. doi:10.1002/wea.97

Blakeslee RJ, Mach DM, Bateman MG, Bailey JC (2014) Seasonal variations in the lightning diurnal cycle and implications for the global electric circuit. Atmos Res 135–136:228–243. doi:10.1016/j.atmosres.2012.09.023

Burns GB, Frank-Kamenetsky AV, Troshichev OA, Bering EA, Reddell BD (2005) Interannual consistency of bi-monthly differences in diurnal variations of the ground-level, vertical electric field. J Geophys Res 110:D10106. doi:10.1029/2004JD005469

Campbell Scientific Inc. (2011) CS110-electric field meter instruction manual. Campbell Scientific Inc, Logan, Utah

Chalmers A (1967) Atmospheric electricity. Pergamon Press Ltd., New York

Chronis TG (2012) Preliminary lightning observations over Greece. J Geophys Res 117:D03113. doi:10.1029/2011JD017063

Conceição R, Melgão M, Silva HG, Nicoll K, Harrison RG, Reis AH (2015) Transport of the smoke plume from Chiado's fire in Lisbon (Portugal) sensed by atmospheric electric field measurements. Air Qual Atmos Heal 0–28. doi: 10.1007/s11869-015-0337-4

Crozier WD (1963) Electrode effect during nighttime low-wind periods. J Geophys Res 68:3451. doi:10.1029/JZ068i011p03451

Defer E, Pinty JP, Coquillat S, Martin JM, Prieur S, Soula S, Richard E, Rison W, Krehbiel P, Thomas R, Rodeheffer D, Vergeiner C, Malaterre F, Pedeboy S, Schulz W, Farges T, Gallin LJ, Ortéga P, Ribaud JF, Anderson G, Betz HD, Meneux B, Kotroni V, Lagouvardos K, Roos S, Ducrocq V, Roussot O, Labatut L, Molinié G (2015) An overview of the lightning and atmospheric electricity observations collected in southern France during the HYdrological cycle in Mediterranean EXperiment (HyMeX), special observation period 1. Atmos Meas Tech 8:649–669. doi:10.5194/amt-8-649-2015

Dolezalek H (1972) Discussion of the fundamental problem of atmospheric electricity. Pure Appl Geophys PAGEOPH 100:8–43. doi:10.1007/BF00880224

Dolezalek H (1992) The world data centre for atmospheric electricity and global change monitoring. European Science Notes Information Bulletin, 92–02. Office of Naval Research–European Office, London

Elhalel G, Yair Y, Nicoll K, Price C, Reuveni Y, Harrison RG (2014) Influence of short-term solar disturbances on the fair weather conduction current. J Sp Weather Sp Clim 4:A26. doi:10.1051/swsc/2014022

García-Talavera M, Quintana B, García-Díez E, Fernández F (2001) Studies on radioactivity in aerosols as a function of meteorological variables in Salamanca (Spain). Atmos Environ 35:221–229. doi:10.1016/S1352-2310(00)00234-X

Georgoulias AK, Papanastasiou DK, Melas D, Amiridis V, Alexandri G (2009) Statistical analysis of boundary layer heights in a suburban environment. Meteorol Atmos Phys 104:103–111. doi:10.1007/s00703-009-0021-z

Guo Y, Barthakur NN, Bhartendu S (1996) Using atmospheric electrical conductivity as an urban pollution indicator. J Geophys Res 101:9197–9203

Harrison RG (2003) Twentieth-century atmospheric electrical measurements at the observatories of Kew, Eskdalemuir and Lerwick. Weather 58:11–19. doi:10.1256/wea.239.01

Harrison RG (2004a) Long-term measurements of the global atmospheric electric circuit at Eskdalemuir, Scotland, 1911–1981. Atmos Res 70:1–19. doi:10.1016/j.atmosres.2003.09.007

Harrison RG (2004b) Long-range correlations in measurements of the global atmospheric electric circuit. J Atmos Solar-Terrestrial Phys 66:1127–1133. doi:10.1016/j.jastp.2004.05.001

Harrison RG (2004c) The global atmospheric electrical circuit and climate. Surv Geophys 25:441–484. doi:10.1007/s10712-004-5439-8

Harrison RG (2006) Urban smoke concentrations at Kew, London, 1898–2004. Atmos Environ 40:3327–3332. doi:10.1016/j.atmosenv.2006.01.042

Harrison RG (2011) Fair weather atmospheric electricity. J Phys Conf Ser 301:012001. doi:10.1088/1742-6596/301/1/012001

Harrison RG (2012) Aerosol-induced correlation between visibility and atmospheric electricity. J Aerosol Sci 52:121–126. doi:10.1016/j.jaerosci.2012.04.011

Harrison RG (2013) The Carnegie curve. Surv Geophys 34:209–232. doi:10.1007/s10712-012-9210-2

Harrison RG, Aplin KL (2002) Mid-nineteenth century smoke concentrations near London. Atmos Environ 36:4037–4043. doi:10.1016/S1352-2310(02)00334-5

Harrison RG, Bennett AJ (2007) Cosmic ray and air conductivity profiles retrieved from early twentieth century balloon soundings of the lower troposphere. J Atmos Solar-Terrestrial Phys 69:515–527. doi:10.1016/j.jastp.2006.09.008

Harrison RG, Carslaw KS (2003) Ion–aerosol–cloud processes in the lower atmosphere. Rev Geophys 41:1–26. doi:10.1029/2002RG000114

Hoppel WA, Anderson RV, Willett JC (1986) Atmospheric electricity in the planetary boundary layer. In: Krider EP, Roble RG (eds) The Earth's electrical environment. National Academy Press, Washington D.C.

Ippolitov II, Kabanov MV, Nagorskii PM, Pkhalagov YA, Smirnov SV (2013) Diurnal variations in the electrical field intensity under smoke from forest fires. Dokl Earth Sci 453:1137–1140. doi:10.1134/S1028334X1311010X

Israelsson S (1978) On the conception "fair weather condition" in atmospheric electricity. Pure Appl Geophys PAGEOPH 116:149–158. doi:10.1007/BF00878989

Israelsson S, Oluwafemi C (1975) Power and cross-power spectral studies of electric and meteorological parameters under fair weather conditions in the atmospheric surface layer. Boundary-Layer Meteorol 9:461–477. doi:10.1007/BF00223394

Israelsson S, Tammet H (2001) Variation of fair weather atmospheric electricity at Marsta Observatory, Sweden, 1993–1998. J Atmos Solar-Terrestrial Phys 63:1693–1703. doi:10.1016/S1364-6826(01)00049-9

Jayaratne ER, Verma TS (2004) Environmental aerosols and their effect on the Earth's local fair-weather electric field. Meteorol Atmos Phys 86:275–280. doi:10.1007/s00703-003-0028-9

Kamra AK (1982) Fair weather space charge distribution in the lowest 2 m of the atmosphere. J Geophys Res 87:4257. doi:10.1029/JC087iC06p04257

King MD, Menzel WP, Kaufman YJ, Tanré D, Gao BC, Platnick S, Ackerman SA, Remer LA, Pincus R, Hubanks PA (2003) Cloud and aerosol properties, precipitable water, and profiles of temperature and water vapor from MODIS. IEEE Trans Geosci Remote Sens 41:442–458. doi:10.1109/TGRS.2002.808226

Kourtidis K, Georgoulias A, Vlahopoulou M, Tsirliganis N, Kastelis N, Ouzounis K, Kazakis N (2015) Radon and radioactivity at a town overlying uranium ores in Northern Greece. J Environ Radioact 150:220–227

Kumar VV, Ramachandran V, Buadromo V, Prakash J (2009) Surface fair-weather potential gradient measurements from a small tropical island station Suva, Fiji. Earth, Planets Sp 61:747–753

Latha R (2003) Diurnal variation of surface electric field at a tropical station in different seasons: a study of plausible influences. Earth, Planets Sp 55:677–685

Latha R (2007) Micrometeorological influences and surface layer radon ion production: consequences for the atmospheric electric field. Atmos Environ 41:867–877. doi:10.1016/j.atmosenv.2006.07.051

Law J (1963) The ionisation of the atmosphere near the ground in fair weather. Q J R Meteorol Soc 89:107–121. doi:10.1002/qj.49708937908

López-Coto I, Mas JL, Bolivar JP (2013) A 40-year retrospective European radon flux inventory including climatological variability. Atmos Environ 73:22–33. doi:10.1016/j.atmosenv.2013.02.043

MacGorman RD, Rust WD (1998) The electrical nature of storms. Oxford University Press, New York

Märcz F, Harrison RG (2003) Long-term changes in atmospheric electrical parameters observed at Nagycenk (Hungary) and the UK observatories at Eskdalemuir and Kew. Ann Geophys 21:2193–2200. doi:10.5194/angeo-21-2193-2003

Marshall TC, Rust WD, Stolzenburg M, Roeder WP, Krehbiel PR (1999) A study of enhanced fair-weather electric fields occurring soon after sunrise. J Geophys Res 104:24455–24469. doi:10.1029/1999JD900418

Mather TA, Harrison RG, Tsanev VI, Pyle DM, Karumudi ML, Bennett AJ, Sawyer GM, Highwood EJ (2007) Observations of the plume generated by the December 2005 oil depot explosions and prolonged fire at Buncefield (Hertfordshire, UK) and associated atmospheric changes. Proc Roy Soc A 463:1153–1177. doi:10.1098/rspa.2006.1810

Mazarakis N, Kotroni V, Lagouvardos K, Argiriou AA (2008) Storms and lightning activity in Greece during the warm periods of 2003–06. J Appl Meteorol Climatol 47:3089–3098. doi:10.1175/2008JAMC1798.1

Moore CB, Vonnegut B, Semonin RG, Bullock JW, Bradley W (1962) Fair-weather atmospheric electric potential gradient and space charge over central Illinois, summer 1960. J Geophys Res 67:1061–1071. doi:10.1029/JZ067i003p01061

Nicoll KA (2012) Measurements of atmospheric electricity aloft. Surv Geophys 33:991–1057. doi:10.1007/s10712-012-9188-9

O'Connor WP (1976) Seasonal changes in diurnal variation of potential gradient at Fargo, North Dakota. Pure Appl Geophys PAGEOPH 114:933–943. doi:10.1007/BF00876193

Pawar S, Gopalakrishnan V, Murugavel P, Sinkevich A, Lal D (2014) Effects of environmental conditions on inducing charge structures of thunderstorms over Eastern India. Earth, Planets Sp 66:54. doi:10.1186/1880-5981-66-54

Pawar SD, Gopalakrishnan V, Murugavel P (2015) Role of orography in inducing high lightning flash rate at the foothills of Himalaya. Earth, Planets Sp 67:51. doi:10.1186/s40623-015-0221-3

Pergamalis F, Papachristopoulos S, Karageorgiou DE, Koukoulis A (1998) Geological features of uranium and rare earths ores of Paranesti Drama areas. In: Proceeding of the 8th International Congress of the Geological Society of Greece, Geological Society of Greece, Patra, May 25–27 1998

Pergamalis F, Karageorgiou ED, Koukoulis A, Katsikis J (2010) Mineralogical-geochemical study of uranium bearing granite phases in Paranesti area, N. Greece. In: Christofides G, Kantiranis N, Kostopoulos DS, Chatzipetros AA (eds) Proceedings of the XIX Congress of the Carpathian–Balkan Geological Association. Spec. Vol. 99, Thessaloniki

Piper IM, Bennett AJ (2012) Observations of the atmospheric electric field during two case studies of boundary layer processes. Environ Res Lett 7:014017. doi:10.1088/1748-9326/7/1/014017

Popov IB, Shvarts YM, Sokolenko LG (2008) Atmospheric electricity measurements on a ground meteorological network of Federal Hydrometeorology and Environmental Monitoring Service (Roshydromet). In: Proceedings of the Technical Conference on Meteorological and Environmental Instruments and Methods of Observation. WMO, St. Petersburg, November 27–29, 2008

Rakov VA, Uman MA (2006) Lightning—physics and effects. Cambridge University Press, Cambridge

Reddell BD, Benbrook JR, Bering EA, Cleary EN, Few AA (2004) Seasonal variations of atmospheric electricity measured at Amundsen–Scott South Pole Station. J Geophys Res 109:1–17. doi:10.1029/2004JA010536

Reiter R (1974) In: Dolezalek H, Reiter R (eds) Atmospheric electricity activities of the Institute for Atmospheric Environmental Research. Proceedings of the Fifth International Conference on Atmospheric Electricity, Garmisch–Partenkirchen

Remer LA, Kaufman YJ, Tanré D, Mattoo S, Chu DA, Martins JV, Li RR, Ichoku C, Levy RC, Kleidman RG, Eck TF, Vermote E, Holben BN (2005) The MODIS aerosol algorithm, products, and validation. J Atmos Sci 62:947–973. doi:10.1175/JAS3385.1

Retalis D (1983) Study of large ions concentration in the air above Athens. Arch Meteorol Geophys Bioclimatol Ser A 32:135–143. doi:10.1007/BF02272718

Retalis D, Retalis A (1997) The atmospheric electric field in Athens–Greece. Meteorol Atmos Phys 63:235–241. doi:10.1007/BF01027388

Retalis A, Nastos P, Retalis D (2009) Study of small ions concentration in the air above Athens, Greece. Atmos Res 91:219–228. doi:10.1016/j.atmosres.2008.05.011

Rycroft M, Israelsson S, Price C (2000) The global atmospheric electric circuit, solar activity and climate change. J Atmos Solar–Terrestrial Phys 62:1563–1576. doi: 10.1016/S1364-6826(00)00112-7

Rycroft MJ, Harrison RG, Nicoll KA, Mareev EA (2008) An overview of earth's global electric circuit and atmospheric conductivity. Space Sci Rev 137:83–105. doi:10. 1007/s11214-008-9368-6

Rycroft MJ, Nicoll KA, Aplin KL, Harrison RG (2012) Recent advances in global electric circuit coupling between the space environment and the troposphere. J Atmos Solar–Terrestrial Phys 90–91:198–211. doi:10.1016/j. jastp.2012.03.015

Sagalyn RC, Faucher GA (1956) Space and time variations of charged nuclei and electrical conductivity of the atmosphere. Q J R Meteorol Soc 82:428–445. doi:10.1002/qj.49708235406

Serrano C, Reis AH, Rosa R, Lucio PS (2006) Influences of cosmic radiation, artificial radioactivity and aerosol concentration upon the fair-weather atmospheric electric field in Lisbon (1955–1991). Atmos Res 81:236–249. doi: 10.1016/j.atmosres.2006.01.001

Sheftel VM, Bandilet OI, Yaroshenko AN, Chernyshev AK (1994) Space–time structure and reasons of global, regional, and local variations of atmospheric electricity. J Geophys Res 99:10797. doi:10.1029/93JD02857

Siingh D, Singh RP, Gopalakrishnan V, Selvaraj C, Panneerselvam C (2013) Fair-weather atmospheric electricity study at Maitri (Antarctica). Earth, Planets Sp 65:1541–1553. doi:10.5047/eps.2013.09.011

Silva HG, Bezzeghoud M, Reis AH, Rosa RN, Tlemĉani M, Araújo AA, Serrano C, Borges JF, Caldeira B, Biagi PF (2011) Atmospheric electrical field decrease during the $M = 4.1$ Sousel earthquake (Portugal). Nat Hazards Earth Syst Sci 11:987–991. doi:10.5194/nhess-11-987-2011

Silva HG, Oliveira MM, Serrano C, Bezzeghoud M, Reis AH, Rosa RN, Biagi PF (2012) Influence of seismic activity on the atmospheric electric field in Lisbon (Portugal) from 1955 to 1991. Ann Geophys 55:193–197. doi:10.4401/ag-5361

Silva HG, Conceição R, Melgão M, Nicoll K, Mendes PB, Tlemçani M, Reis AH, Harrison RG (2014) Atmospheric electric field measurements in urban environment and the pollutant aerosol weekly dependence. Environ Res Lett 9:114025. doi:10.1088/1748-9326/9/11/114025

Smirnov S (2014) Reaction of electric and meteorological states of the near-ground atmosphere during a geomagnetic storm on 5 April 2010. Earth, Planets Sp 66: 154. doi:10.1186/s40623-014-0154-2

Takagi M, Iwata A (1980) A seasonal effect in diurnal variation of the atmospheric electric field on the Pacific coast of Japan. Pure Appl Geophys PAGEOPH 118: 953–963. doi:10.1007/BF01593042

Tammet H (2009) A joint dataset of fair-weather atmospheric electricity. Atmos Res 91:194–200. doi:10.1016/j.atmosres.2008.01.012